INFLAMMATION

Depletion of H_2S during obesity enhances store-operated Ca^{2+} entry in adipose tissue macrophages to increase cytokine production

Gopal V. Velmurugan,[1][*] Huiya Huang,[1][*] Hongbin Sun,[1] Joseph Candela,[1]
Mukesh K. Jaiswal,[2] Kenneth D. Beaman,[2] Megumi Yamashita,[3]
Murali Prakriya,[3] Carl White[1][†]

The increased production of proinflammatory cytokines by adipose tissue macrophages (ATMs) contributes to chronic, low-level inflammation during obesity. We found that obesity in mice reduced the bioavailability of the gaseous signaling molecule hydrogen sulfide (H_2S). Steady-state, intracellular concentrations of H_2S were lower in ATMs isolated from mice with diet-induced obesity than in ATMs from lean mice. In addition, the intracellular concentration of H_2S in the macrophage cell line RAW264.7 was reduced during an acute inflammatory response evoked by the microbial product lipopolysaccharide (LPS). Reduced intracellular concentrations of H_2S led to increased Ca^{2+} influx through the store-operated Ca^{2+} entry (SOCE) pathway, which was prevented by the exogenous H_2S donor GYY4137. Furthermore, GYY4137 inhibited the Orai3 channel, a key component of the SOCE machinery. The enhanced production of proinflammatory cytokines by RAW264.7 cells and ATMs from obese mice was reduced by exogenous H_2S or by inhibition of SOCE. Together, these data suggest that the depletion of macrophage H_2S that occurs during acute (LPS-induced) or chronic (obesity) inflammation increases SOCE through disinhibition of Orai3 and promotes the production of proinflammatory cytokines.

INTRODUCTION

The increased abundance of inflammatory markers and of proinflammatory cytokines in the circulation are hallmarks of obesity (1–3). This state of chronic, low-level inflammation is associated with insulin resistance (3–5) and also predicts the future development of type 2 diabetes (6) and cardiovascular disease (1, 7). The point of origin of proinflammatory cytokine production in obesity has been localized to an increased population of macrophages that are recruited to visceral fat deposits (2, 8). These adipose tissue macrophages (ATMs) have a degree of plasticity that enables them to adopt either a proinflammatory (defined as M1) or an anti-inflammatory (M2) phenotype. Although any given cell is likely to reside somewhere along a spectrum of activation from M1 to M2, the consensus is that, during obesity, the balance is tilted toward the proinflammatory M1 phenotype (9). A major challenge in the field is to identify the signal transduction pathways modulated by obesity and define the importance of this modulation on maintaining the M1 phenotype in ATMs.

The gaseous signaling molecule hydrogen sulfide (H_2S) has been identified as an important inflammatory mediator (10–15). That H_2S has an anti-inflammatory function in macrophages is supported by the observation that experimental application of H_2S donors to primary macrophages (16) and macrophage cell lines (10, 13) robustly attenuates cytokine production evoked by proinflammatory stimuli. These findings are particularly intriguing in light of data that point to impaired H_2S signaling in type 2 diabetes (17–19) and show depleted plasma concentrations of H_2S in human obesity (20). This raises the possibility that the depletion of endogenous H_2S is involved in driving ATMs toward the M1 phenotype. The question arises then as to how a reduction in H_2S results in increased proinflammatory signaling.

A robust Ca^{2+} signal is an essential component of the proinflammatory cascade in macrophages (21, 22), and its generation is likely to be heavily dependent on the activity of the store-operated Ca^{2+} entry (SOCE) pathway (23–25). In immune cells, SOCE is mediated by the Ca^{2+} release–activated Ca^{2+} (CRAC) channels, which are activated in response to the depletion of endoplasmic reticulum (ER) stores of Ca^{2+} (26). The SOCE machinery consists of the ER-localized stromal interaction molecule (STIM), which, upon store depletion, binds to and opens Orai, the plasma membrane pore-forming subunit of the CRAC channel (27–29). Although H_2S inhibits Ca^{2+} influx through several different plasmalemmal ion channels (30), whether H_2S impinges on SOCE by targeting CRAC channels is unclear. If H_2S were an inhibitor of SOCE, then a downstream consequence of its action would be the attenuation of cytokine production by limiting Ca^{2+} influx during proinflammatory signaling. Similarly, if endogenous H_2S production were compromised, then enhanced cytokine production would be expected to occur because of disinhibited SOCE. Such a model would be consistent with the known anti-inflammatory function of H_2S in macrophages.

Which components of the proinflammatory signaling pathway are targeted by H_2S in macrophages is unclear. Whether H_2S homeostasis is affected by obesity or, indeed, if disrupted H_2S homeostasis contributes to chronic, low-level inflammation during obesity is unknown. We hypothesized that obesity disrupts a H_2S-Ca^{2+} signaling axis to amplify the proinflammatory cascade, which has implications for obesity-dependent inflammation. This hypothesis was tested in RAW264.7 cells (a mouse macrophage cell line) and in primary mouse macrophages by quantifying H_2S concentrations, SOCE, and cytokine production in response to proinflammatory stimuli or diet-induced obesity.

[1]Department of Physiology and Biophysics, Chicago Medical School, Rosalind Franklin University of Medicine and Science, North Chicago, IL 60064, USA. [2]Department of Microbiology and Immunology, Chicago Medical School, Rosalind Franklin University of Medicine and Science, North Chicago, IL 60064, USA. [3]Department of Pharmacology, Feinberg School of Medicine, Northwestern University, Chicago, IL 60611, USA.
[*]These authors contributed equally to this work.
[†]Corresponding author. E-mail: carl.white@rosalindfranklin.edu

RESULTS

### Endogenous H₂S is depleted in ATMs isolated from obese mice

The abundances of mRNAs of well-characterized pro- and anti-inflammatory markers were assessed to define the inflammatory phenotype of ATMs isolated from lean and obese mice. Consistent with previous studies, the mRNAs of proinflammatory M1 markers, including nitric oxide synthase 2, inducible (*NOS2*) and integrin α X (*ITGAX*; also known as CD11c), were increased in abundance, whereas the mRNAs of anti-inflammatory M2 markers, including mannose receptor C type 1 (*MRC1*), arginase 1 (*ARG1*), and chitinase-like 3 (*Chil3*; also known as Ym1), were decreased in abundance in ATMs from obese mice compared to those in ATMs from lean control mice (Fig. 1, A and B). The endogenous, basal intracellular concentration of H₂S was then quantified in single cells loaded with the H₂S-specific fluorescent probe SF7-AM. This latest generation probe is highly specific for H₂S and is insensitive to other reactive sulfur, oxygen, and nitrogen species, and it has been validated as a tool to measure qualitative changes in intracellular H₂S concentrations (*31, 32*). This approach revealed that the steady-state H₂S concentration in ATMs from obese mice was substantially less than that in ATMs from lean mice (Fig. 1, C and D). Because H₂S production is highly dependent on the enzyme cystathionine γ-lyase (CSE), we determined its abundance in ATMs from lean and obese mice. We found that there was a consistent and marked increase in the amounts of CSE mRNA and protein in ATMs from the obese mice (Fig. 1, E and F). Induction of expression of the gene encoding CSE in response to diverse inflammatory stimuli was described previously (*33–35*); however, we observed that the concentration of endogenous H₂S was substantially decreased despite the increased abundance of CSE. The ability of CSE in whole-cell lysates from the fat pads of lean and obese mice to produce H₂S was assessed with the methylene blue technique (*36*) and the maximal H₂S production capacity found to be increased by obesity (Fig. 1G).

### Proinflammatory stimulation decreases the amount of H₂S in macrophages

The relationship between macrophage activation status, CSE abundance, and H₂S concentration was further explored in experiments with RAW264.7 cells. The cells were challenged with lipopolysaccharide (LPS) to evoke a robust proinflammatory signaling cascade, which induces CSE production (*33*). Stimulation of RAW264.7 cells with LPS resulted in a substantial reduction in the intracellular concentration of H₂S (Fig. 2, A and B), which is consistent with our observations of ATMs from lean and obese mice. Similarly, the decrease in H₂S concentration occurred despite there being an increase in the abundance of CSE protein, whereas the abundance of cystathionine β-synthase (CBS), another enzyme capable of generating H₂S, was unaffected by LPS (Fig. 2C and fig. S1). In a parallel set of experiments, cells were preincubated with the exogenous H₂S donor GYY4137 before being treated with LPS or vehicle. GYY4137 is a slow-releasing H₂S donor that results in a sustained increase in the amount of H₂S (*37*). As expected, the concentration of H₂S was increased in cells incubated with GYY4137 alone; however, in the presence of GYY4137, LPS had no effect on the H₂S concentration (Fig. 2, A and B). Thus, GYY4137 effectively maintained the cellular concentration of H₂S during proinflammatory stimulation. Furthermore, the addition of the CSE substrate ʟ-cysteine to the cells also prevented the LPS-induced decease in the concentration of H₂S (Fig. 2B).

We next assessed the enzymatic function of CSE by measurement of maximal H₂S production with the methylene blue technique. RAW264.7 cells were treated with LPS or vehicle for 4 hours, and then their H₂S-

producing capacity was measured. The capacity to produce H₂S was almost doubled in response to LPS (Fig. 2D). These data suggest that LPS induces the production of functional CSE protein. Thus, the observed
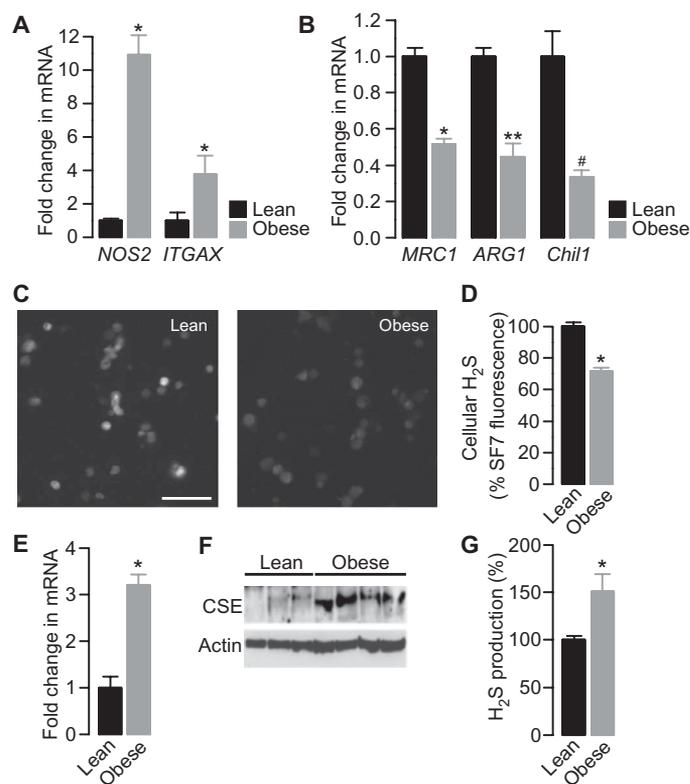
Fig. 1. Increased proinflammatory markers in ATMs from obese mice that exhibit decreased cellular H₂S concentrations correlate with increased CSE abundance and H₂S production capacity compared to ATMs from lean controls. (**A** and **B**) ATMs isolated from lean and obese mice were analyzed by quantitative reverse-transcription polymerase chain reaction (qRT-PCR) to determine the relative abundances of mRNAs encoding the classical M1 activation markers *NOS2* and *ITGAX* (A) and the M2 activation markers *MRC1*, *ARG1*, and *Chil3* (B). Data are expressed as the mean fold difference ± SEM in mRNA abundance between ATMs from three mice of each group. *$P < 0.001$, **$P = 0.003$, #$P = 0.04$ by unpaired t test. (**C**) Representative fluorescence images showing ATMs from lean (left) and obese (right) mice loaded with the H₂S indicator SF7-AM. Scale bar, 50 μm. Images are representative of three mice of each group. (**D**) Quantification of the SF7-AM fluorescence in single ATMs taken from three lean and three obese mice. Data are means ± SEM and expressed as a percentage of the SF7-AM fluorescence measured in ATMs from lean mice. Statistical analysis was performed before data were normalized. *$P < 0.001$ by unpaired t test. (**E**) ATMs from lean and obese mice were analyzed by qRT-PCR to determine the relative abundance of *CSE* mRNA. Data are the mean fold differences in mRNA abundance ± SEM in ATMs between lean and obese mice and are from independent samples prepared from three lean and four obese mice. *$P < 0.001$ by unpaired t test. (**F**) ATMs isolated from three lean and four obese mice were analyzed by Western blotting to detect CSE. Actin was used as a loading control. (**G**) Epididymal fat pad lysates from five lean and five obese mice were analyzed by the methylene blue technique to determine the extent of H₂S production. Data are means ± SEM and are expressed as a percentage of the amount of H₂S produced in samples from lean mice. *$P < 0.001$ by unpaired t test.
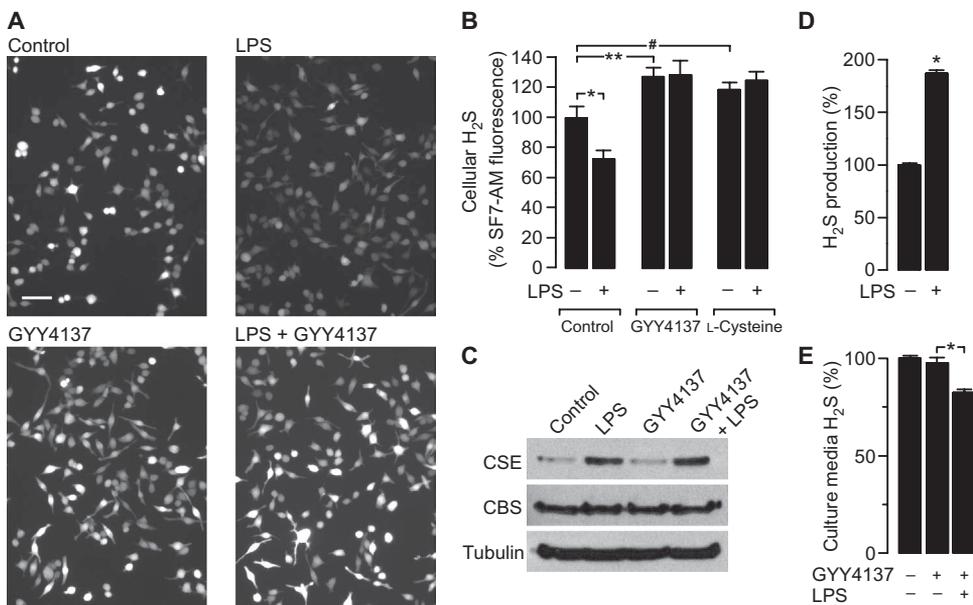
Fig. 2. LPS decreases the cellular concentration of H_2S while increasing CSE abundance and H_2S production capacity in RAW264.7 cells. (A) RAW264.7 cells loaded with the H_2S indicator SF7-AM were pretreated with 500 µM GYY4137 or vehicle before being incubated for 4 hours with either vehicle (control) or LPS (1 µg/ml). Cells were then analyzed by fluorescence microscopy. Images are representative of six independent experiments. When used, GYY4137 was present throughout the entire incubation period. Scale bar, 50 µm. (B) Analysis of SF7-AM fluorescence data. Data are means ± SEM of the SF7-AM fluorescence intensities of individual cells expressed as a percentage of control, untreated cells. Data are from single cells and were pooled from six independent samples. $*P = 0.017$, $**P = 0.012$, $#P = 0.016$ by one-way analysis of variance (ANOVA). (C) RAW264.7 cells were pretreated with vehicle or 500 µM GYY4137 before being incubated for 4 hours with vehicle or LPS (1 µg/ml). Cells were then analyzed by Western blotting with antibodies against the indicated proteins. Western blots are representative of three independent experiments. For quantification of band intensities, see fig. S1. (D) RAW264.7 cells were incubated for 4 hours with vehicle or LPS (1 µg/ml). Cell lysates were then analyzed by the methylene blue technique to detect H_2S. Data are expressed as a percentage of the H_2S measured in untreated cell lysates and are means ± SEM of five experiments. $*P < 0.001$ by unpaired t test. (E) RAW264.7 cell cultures were left untreated or were treated overnight with 50 µM GYY4137 in the absence or presence of LPS (1 µg/ml). Cell culture medium was then analyzed by the methylene blue technique to determine the concentration of H_2S. Data were normalized to the amount of H_2S measured in cell-free medium. Data are expressed as a percentage of the H_2S found in the culture medium of untreated cells and are means ± SEM of five experiments.

sensitive to the application of exogenous H_2S, and it should be modified in response to changes in the abundance of endogenous H_2S caused by proinflammatory conditions. This was tested in experiments with macrophages with a well-established approach to quantify SOCE (38). In this protocol, the ER stores of Ca^{2+} are first depleted in the absence of extracellular Ca^{2+} by inhibiting the sarco/endoplasmic reticulum Ca^{2+}-ATPase (SERCA) pump with cyclopiazonic acid (CPA). When Ca^{2+} is then added back to the culture medium, it enters the cell through the activated SOCE channels. Thus, the amplitude of the Ca^{2+} influx reflects the activation status of SOCE. By measuring intracellular Ca^{2+} with live-cell Ca^{2+} imaging, we found that the magnitude of SOCE recorded in RAW264.7 cells was substantially increased in response to LPS (Fig. 3, A to C). Although GYY4137 had no effect on SOCE in unstimulated cells, it completely blocked the increase in SOCE evoked by LPS (Fig. 3, A to C). To further validate these observations, the same experiments were performed with freshly isolated mouse peritoneal macrophages. Qualitatively similar results were obtained, in that GYY4137 blocked the LPS-induced increase in SOCE; however, in contrast to its effect on RAW264.7 cells, GYY4137 reduced SOCE in unstimulated macrophages (Fig. 3, D to F). Neither LPS nor GYY4137 altered the basal cytoplasmic concentration of Ca^{2+} or the steady-state ER store content in either RAW264.7 cells (Fig. 3, A and B) or peritoneal macrophages (Fig. 3, D and E). SOCE in macrophages is mediated by the STIM-Orai machinery (26). We therefore quantified the amounts of all STIM and Orai proteins in control and LPS-stimulated RAW264.7 cells in the presence and absence of GYY4137 (Fig. 3G and fig. S2). Protein abundance was unaffected by LPS or GYY4137, suggesting that H_2S affects SOCE function in macrophages by physiological modulation, in contrast to lymphocytes in which the abundances of STIM and Orai proteins are increased in response to T cell receptor engagement (39).

SOCE is inhibited by H_2S
Increased SOCE correlated with decreased H_2S concentrations in LPS-stimulated cells. If H_2S directly regulated SOCE activity, then we would expect SOCE to increase in response to H_2S depletion, even in the absence of LPS. The endogenous production of H_2S in macrophages is largely dependent on the activity of CSE and, to a lesser extent, CBS (15, 40). To examine the contribution of endogenous H_2S to the regulation of SOCE, we inhibited CSE and CBS with DL-propargylglycine (PPG) and aminooxyacetic acid (AOAA), respectively (41). Treatment of RAW264.7 cells with both PPG and AOAA substantially reduced the cellular concentration of H_2S (Fig. 4, A and B), which was associated with an increase in the magnitude of SOCE in both RAW264.7 cells (Fig. 4, C and D) and

decrease in cellular H_2S concentration in response to LPS was unlikely a result of a loss in CSE function. We therefore asked whether increased H_2S consumption could account for the apparent paradox. This was assessed in experiments in which RAW264.7 cells were stimulated overnight with LPS in the absence or presence of GYY4137 before the concentration of H_2S in the cell culture medium was determined with the methylene blue technique. Measurements were normalized to control samples drawn from culture wells containing GYY4137 but no cells. A reduction in the concentration of H_2S was observed only in medium from cell cultures that were treated with LPS (Fig. 2E). Thus, increased cellular demand for and consumption of H_2S may well account for the LPS-induced depletion of H_2S from the cell culture medium.

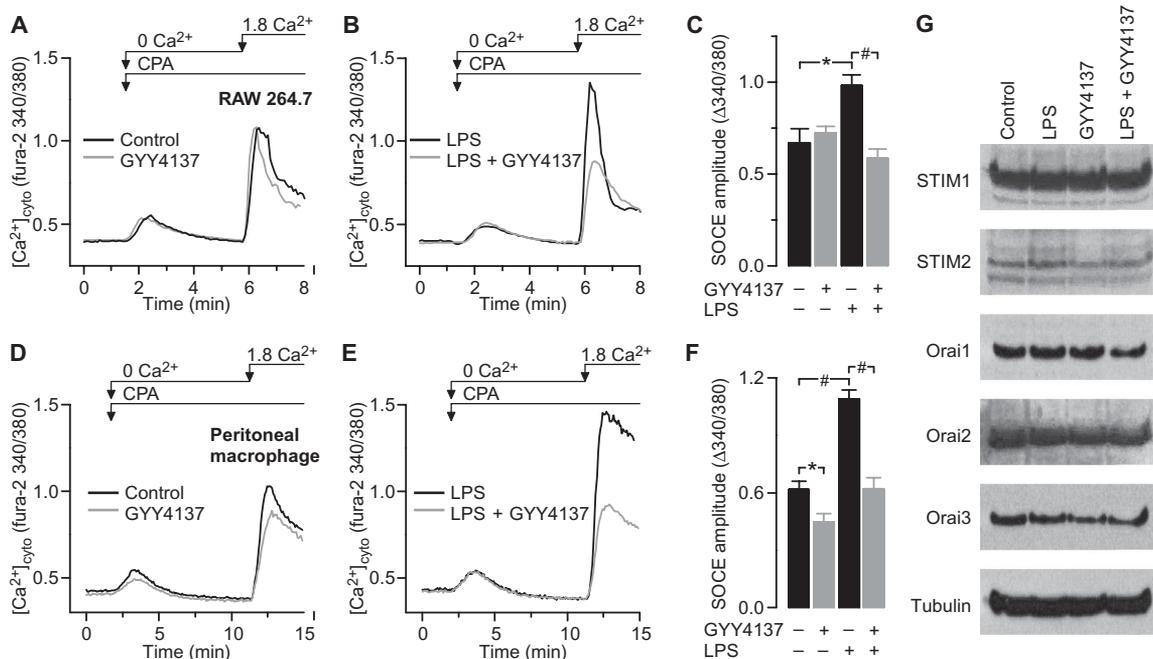## Proinflammatory stimulation increases SOCE in macrophages
We postulated that the SOCE pathway was an important physiological target of H_2S. If this was correct, the magnitude of SOCE should be

Fig. 3. GYY4137 blocks the LPS-induced increase in SOCE. (A to F) Analysis of cytosolic Ca^{2+} flux in RAW264.7 cells and freshly isolated mouse peritoneal macrophages. To activate maximal SOCE, ER stores were depleted by the application of 10 μM CPA in the absence of extracellular Ca^{2+}. Note that the area under the transient increase in $[Ca^{2+}]_{cyto}$ in response to CPA is an index of resting ER store content, whereas the amplitude of the Ca^{2+} spike evoked upon adding Ca^{2+} back to the buffer reflects the magnitude of SOCE. (A) Typical traces recorded in RAW264.7 cells and depicting SOCE in the presence or absence of 500 μM GYY4137. (B) Measurement of SOCE in RAW264.7 cells treated for 4 hours with LPS (1 μg/ml) in the absence or presence of 500 μM GYY4137. (C) SOCE amplitudes in RAW264.7 cells treated under the indicated conditions. Data are means ± SEM of five to eight independent experiments. *P = 0.005, #P < 0.001 by one-way ANOVA. (D) Typical traces recorded in mouse peritoneal macrophages and depicting SOCE in the presence or absence of 500 μM GYY4137. (E) Traces showing SOCE recorded in peritoneal macrophages after stimulation with LPS (1 μg/ml) in the absence or presence of 500 μM GYY4137. (F) SOCE amplitude in peritoneal macrophages treated under the indicated conditions. Data are means ± SEM of five to seven independent experiments. *P = 0.029, #P < 0.001 by one-way ANOVA. (G) RAW264.7 cells were treated for 4 hours with the indicated combinations of vehicle, LPS (1 μg/ml), or 500 μM GYY4137. Cells were then analyzed by Western blotting with antibodies against the indicated proteins. Western blots are representative of three independent experiments. For quantification of band intensities, see fig. S2.

mouse peritoneal macrophages (fig. S3, A and B). The involvement of CSE was further explored through a short hairpin RNA (shRNA)–based knockdown approach. RAW264.7 cells stably expressing either control shRNA or CSE-specific shRNA were generated, and knockdown of CSE was confirmed by Western blotting analysis (fig. S3, C and D). Consistent with the pharmacological experiments, the steady-state concentration of H_2S was lower in CSE knockdown cells than in control cells (Fig. 4, E and F). Similarly, SOCE was increased in cells in which CSE was knocked down (Fig. 4, G and H). Together, these data are consistent with a model in which cellular H_2S normally limits the maximal extent of SOCE.

## Both H_2S and SOCE determine the magnitude of proinflammatory cytokine production

Proinflammatory stimulation of macrophages by LPS ultimately results in the release of a range of inflammatory cytokines, including interleukin-6 (IL-6) and IL-1β. Because transcription of the genes encoding these molecules is tightly linked to the strength of the accompanying Ca^{2+} signal (21, 22), we postulated that H_2S was anti-inflammatory by virtue of its inhibitory effect on SOCE. We therefore examined the relationship between H_2S, SOCE, and cytokine production. As expected, LPS induced the expression of *IL6* and *IL1B* as assessed by qRT-PCR assays (Fig. 5A), an effect that was attenuated in the presence of the H_2S donor GYY4137 (Fig. 5B), consistent with previous observations (13). To establish the relevance of the SOCE pathway for cytokine production, SOCE was targeted both pharmacologically and genetically (Fig. 5, C to H). Treatment of RAW264.7 cells with *N*-[4-[3,5-*bis*(trifluoromethyl)-1*H*-pyrazol-1-yl]phenyl]-4-methyl-1,2,3-thiadiazole-5-carboxamide (BTP2), a SOCE inhibitor (42), effectively inhibited SOCE (Fig. 5, C and D) as did the knockdown of STIM1 with specific small interfering RNA (siRNA) (Fig. 5, F and G, and fig. S4). Both approaches were equally effective at reducing the amounts of proinflammatory cytokines produced in response to LPS (Fig. 5, E and H). Thus, approaches that limited the magnitude of SOCE, whether by H_2S-dependent inhibition (Fig. 3), by pharmacological blockade of SOCE (Fig. 5C), or by knockdown of STIM1 (Fig. 5F), were all effective at dampening the transcriptional activity of genes encoding key proinflammatory molecules.

Obesity is associated with increased SOCE and cytokine production in ATMs, which are dependent on the depletion of H_2S

We showed that H_2S was depleted in ATMs during obesity (Fig. 1) and that the depletion of H_2S resulted in increased SOCE in macrophages (Fig. 3). If H_2S depletion and the accompanying loss of SOCE inhibition were universal features of the proinflammatory M1 phenotype, then we would predict that SOCE would be increased in ATMs from obese mice. We therefore assessed SOCE in ATMs isolated from lean and obese mice and found, as expected, that SOCE was markedly increased in cells from the obese mice (fig. S5, A to C). The mean steady-state concentration of Ca^{2+} in ER stores was slightly increased in ATMs from obese mice but was not statistically significantly different (fig. S5D). In contrast, the ATMs from obese animals exhibited increased basal concentrations of cytosolic Ca^{2+} (fig. S5E). However, because this
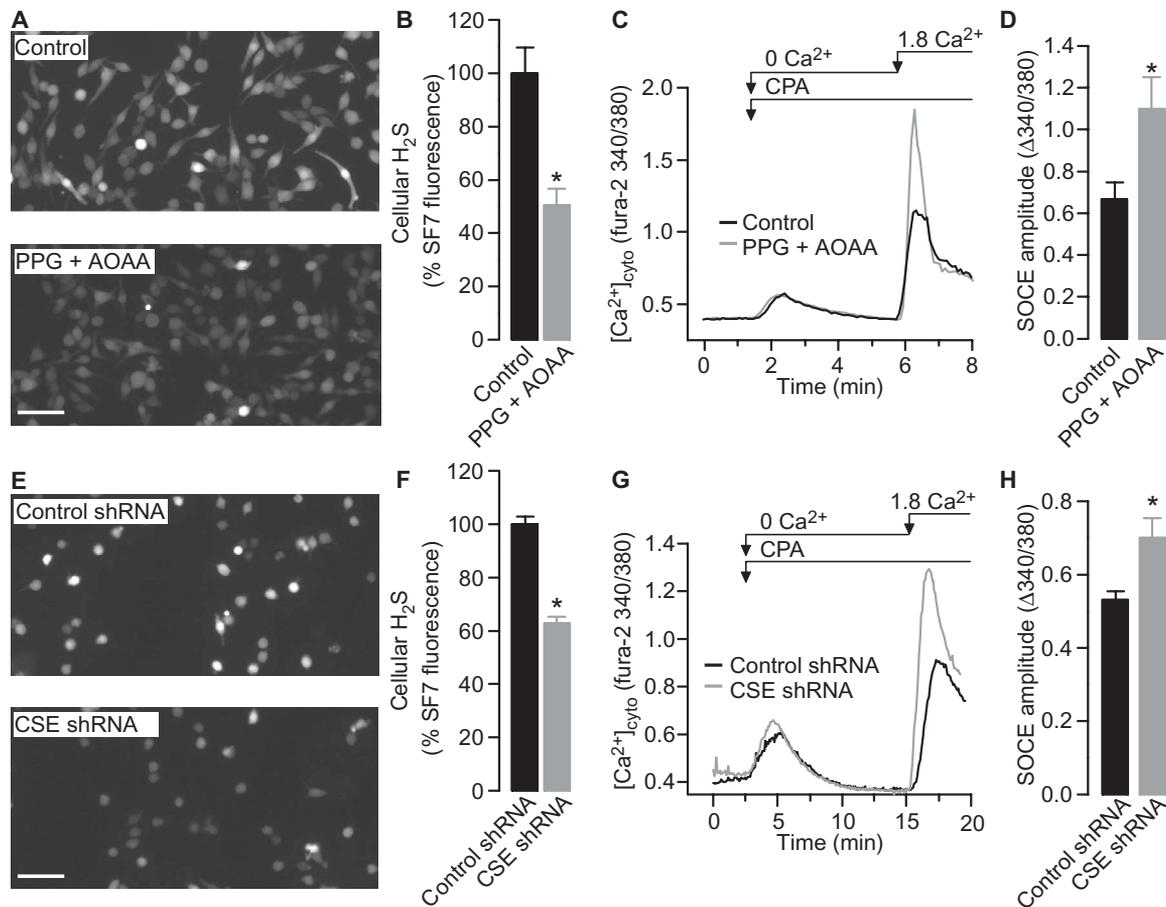
Fig. 4. Inhibition of H$_2$S production increases SOCE in unstimulated RAW264.7 cells. (A) RAW264.7 cells loaded with the H$_2$S indicator SF7-AM were incubated for 1 hour either with vehicle control (top) or with 0.4 mM PPG and 0.4 mM AOAA (bottom). Cells were then analyzed by fluorescence microcopy. Images are representative of six independent experiments. Scale bar, 50 μm. (B) Quantification of the SF7-AM fluorescence in RAW264.7 cells. Data are means ± SEM of the SF7-AM fluorescence intensities of individual cells expressed as a percentage of control cells from six independent experiments. *P = 0.005 by unpaired t test. (C) Typical SOCE traces in RAW264.7 cells in the presence or absence of both PPG and AOAA were recorded as described in Fig. 3A. (D) SOCE amplitudes in RAW264.7 cells in the presence or absence of both PPG and AOAA. Data are means ± SEM of five to seven independent experiments. *P = 0.023 by unpaired t test. (E) RAW264.7 cells stably expressing control shRNA (top) or CSE-specific shRNA (bottom) were loaded with the H$_2$S indicator SF7-AM. Cells were then analyzed by fluorescence microcopy. Images are representative of four independent experiments. Scale bar, 50 μm. (F) Quantification of the effect of CSE knockdown on SF7-AM fluorescence in RAW264.7 cells. Data are means ± SEM of the SF7-AM fluorescence intensities of individual cells expressed as a percentage of control cells from four independent experiments. *P < 0.001 by unpaired t test. (G) Typical SOCE traces in RAW264.7 cells treated with control shRNA or CSE-specific shRNA were recorded as described in Fig. 3A. (H) Effect of CSE knockdown on SOCE amplitudes in RAW264.7 cells. Data are means ± SEM of five independent experiments. *P = 0.015 by unpaired t test.

was not also observed in RAW264.7 cells, peritoneal macrophages, or ATMs from lean mice in which SOCE was increased by CSE inhibition, we conclude that this observation was unlikely to be related to the increased SOCE.

We next asked whether the obesity-dependent increase in SOCE observed in ATMs was caused by H$_2$S depletion. We tested this by monitoring SOCE in ATMs after treatment with either the H$_2$S donor GYY4137 or the CSE and CBS inhibitors PPG and AOAA. GYY4137 reduced the obesity-dependent increase in SOCE such that it was similar to the extent of SOCE observed in ATMs from the lean animals (Fig. 6, A to C). The rescue of SOCE by exogenous H$_2$S is consistent with our hypothesis that depletion of endogenous H$_2$S causes increased SOCE in obesity. This hypothesis was further supported by the observation that inhibition of endog-

enous H$_2$S production by PPG and AOAA increased the extent of SOCE in ATMs from lean mice but produced no further increase in SOCE in ATMs from obese mice (Fig. 6C).

We next investigated whether the depletion of endogenous H$_2$S during obesity was an important contributor to increased cytokine production and if this were likely mediated by its influence on SOCE. Freshly isolated ATMs were cultured in the absence or presence of GYY4137 or BTP2, separately or in combination. We could not use qRT-PCR analysis in these experiments because of the limited cell numbers available; however, cytokine concentrations in the culture medium were measured 24 hours after plating. In the absence of any treatment, the amounts of IL-6, IL-1β, and TNF-α secreted by ATMs from obese mice were substantially greater than those produced by ATMs from lean control mice (Fig. 6, D to F),
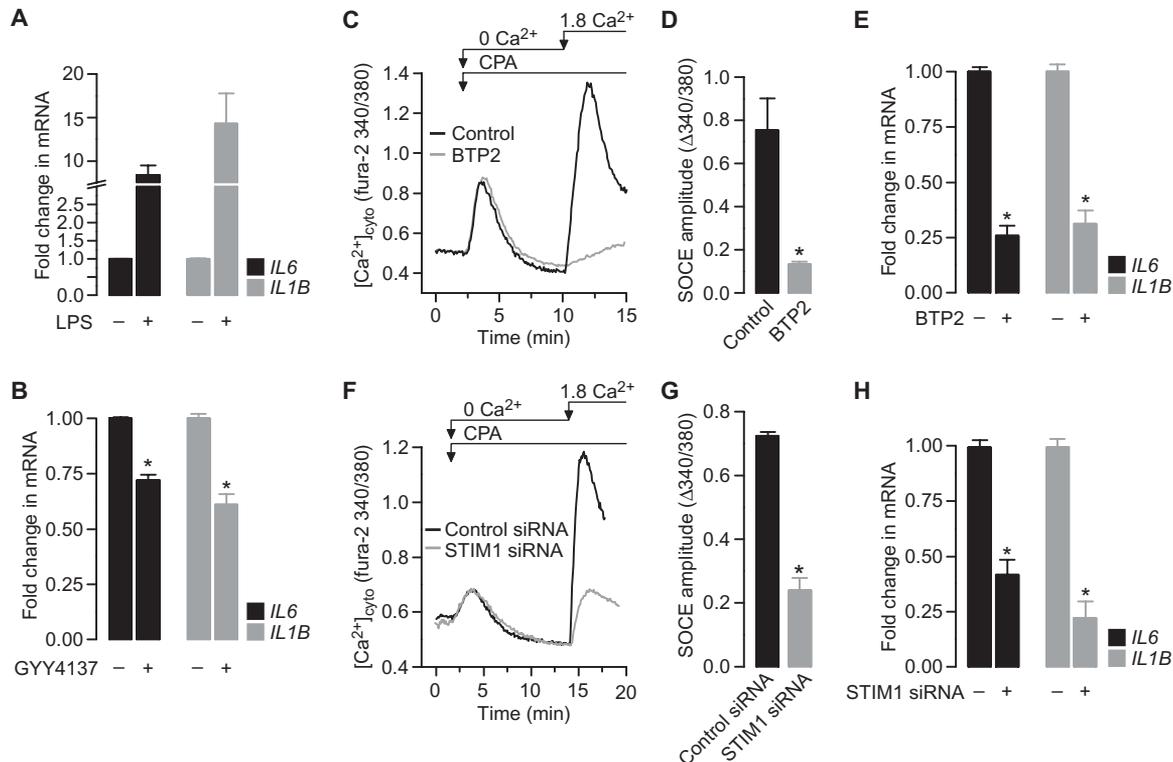
Fig. 5. Increasing the cellular concentration of H_2S or inhibiting SOCE attenuates proinflammatory cytokine production by LPS-treated RAW264.7 cells. (**A**) RAW264.7 cells were treated for 4 hours with vehicle or LPS (1 µg/ml) before being analyzed by qRT-PCR to determine the relative abundances of the indicated mRNAs. (**B**) RAW264.7 cells treated for 4 hours with LPS (1 µg/ml) in the presence or absence of 500 µM GYY4137 were analyzed by qRT-PCR to determine the relative abundances of the indicated mRNAs. (**C**) Typical SOCE traces in RAW264.7 cells in the presence or absence of 10 µM BTP2 were recorded as described in Fig. 3A. (**D**) SOCE amplitudes in RAW264.7 cells in the presence or absence of BTP2.

(**E**) RAW264.7 cells treated for 4 hours with LPS (1 µg/ml) in the presence or absence of 10 µM BTP2 were analyzed by qRT-PCR to determine the relative abundances of the indicated mRNAs. (**F**) Typical SOCE traces in RAW264.7 cells treated with control siRNA or STIM1-specfic siRNA were recorded as described in Fig. 3A. (**G**) SOCE amplitudes in RAW264.7 cells treated with control siRNA or STIM1-specfic siRNA. (**H**) RAW264.7 cells treated with control siRNA or STIM1-specific siRNA were analyzed by qRT-PCR to determine the relative abundances of the indicated mRNAs. Data in all bar charts are means ± SEM of at least three independent experiments. *$P < 0.001$ by unpaired t test.

as expected. The presence of either GYY4137 or BTP2 attenuated cytokine production by ATMs from the obese mice, although statistical significance was not always achieved (Fig. 6, E and F). Only IL-6 production by ATMs was statistically significantly reduced by either GYY4137 or BTP2. Neither GYY4137 nor BTP2 affected the amounts of cytokines produced by ATMs from lean mice, with the exception of IL-6, which saw decreased production in the presence of both GYY4137 and BTP2 (Fig. 6D).

H_2S selectively targets Orai3

How then does H_2S regulate SOCE? The ER-localized STIM molecules sense store depletion and activate Ca^{2+} influx by binding to and opening the plasma membrane Orai channels (*43*). It was therefore conceivable that H_2S could inhibit SOCE by influencing the function of STIM or Orai proteins. To identify the specific target of H_2S, we examined the effects of H_2S on the function of SOCE in human embryonic kidney (HEK) 293 cells transiently transfected with fluorescently tagged STIM and Orai proteins. Previous studies showed that the exogenous expression of these proteins in HEK 293 cells effectively reconstitutes SOCE, whose magnitude is greatly enhanced, enabling the functional characterization of specific Orai isoforms with minimal contamination from endogenous channels (*44–46*).

We transiently transfected HEK 293 cells stably expressing STIM1 with plasmids encoding Orai1, Orai2, or Orai3 (fig. S6) and then measured SOCE. Treatment of these cells with the H_2S donor GYY4137 had no effect on SOCE mediated by Orai1 or Orai2 but markedly reduced SOCE in cells expressing Orai3 (Fig. 7, A and B).

The Ca^{2+} imaging data suggested that H_2S specifically affected SOCE mediated by STIM1 and Orai3. In principle, there are several possible mechanisms, both direct and indirect, that could account for this effect of H_2S. These include changes in the abundance or function of CRAC channel proteins, as well as mechanisms involving membrane depolarization that reduce the electrochemical gradient for Ca^{2+} entry. To further assess the effect of H_2S on Orai3-mediated SOCE, we used patch clamp electrophysiology to directly measure CRAC currents in HEK 293 cells that stably expressed STIM1 and were transiently transfected with plasmid encoding Orai3. Administration of the H_2S donor GYY4137 decreased Orai3-dependent currents but did not alter the current-voltage relationship, indicating that H_2S inhibited Orai3 channel activity without altering its ion selectivity (Fig. 7, C and D). These data are consistent with a model in which H_2S directly affects SOCE by inhibiting CRAC currents mediated by STIM1 and Orai3.
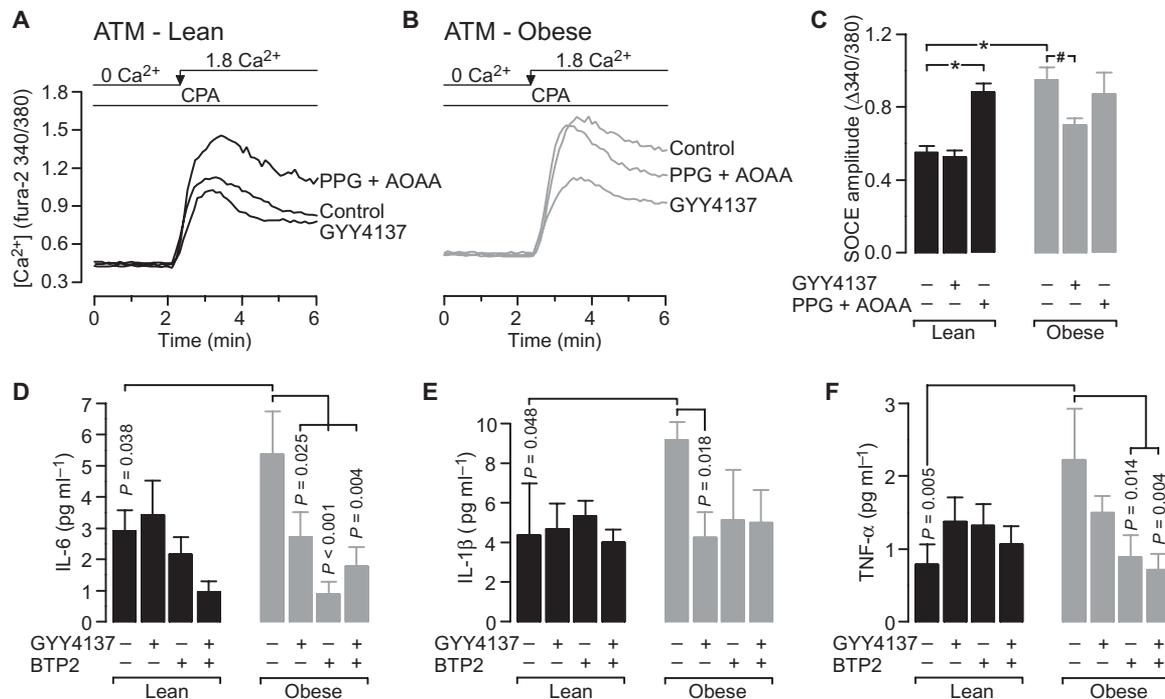
Fig. 6. Increased SOCE during obesity is dependent on the depletion of H$_2$S and is associated with increased proinflammatory cytokine production. (A and B) Typical recordings of SOCE in ATMs from lean mice (A) and obese mice (B). For clarity, only the Ca^{2+} readdition portion of the experiment is shown, and it depicts SOCE evoked in cells treated with vehicle, 500 μM GYY4137, or both 0.4 mM PPG and 0.4 mM AOAA. (C) SOCE amplitudes in ATMs from lean and obese mice treated with vehicle, GYY4137, or PPG/AOAA. Data are means ± SEM of six to eight independent sam-

ples derived from three lean and three obese mice. *$P < 0.001$, #$P = 0.016$ by unpaired t test. (D to F) ATMs isolated from lean or obese mice were plated and cultured overnight in the presence of the indicated combinations of vehicle, 500 μM GYY4137, and 10 μM BTP2. The concentrations of IL-6 (D), IL-1β (E), and TNF-α (tumor necrosis factor–α) (F) in the cell culture medium were then measured by Luminex assay. Data are means ± SEM of independent cultures derived from seven lean and seven obese mice. P values were determined by one-way ANOVA analysis.

All experimental assays examining the effect of GYY4137 on SOCE were performed after the cells were incubated with GYY4137 for 1 hour. To assess the time course of the effect of H$_2$S on SOCE, the SOCE measurement protocol was initiated at various time points after the addition of GYY4137 (Fig. 7E). These data suggest that the inhibitory action of H$_2$S on SOCE was complete within 20 to 40 min. Finally, we examined the functional importance of Orai3 in regulating cytokine production using a knockdown strategy in RAW264.7 cells. Cells were treated with control or Orai3-specific siRNAs, and Orai3 knockdown was confirmed by Western blotting analysis (fig. S7). Next, we assessed the LPS-induced expression of *IL6* and *IL1B* by qRT-PCR analysis (Fig. 7F). We found that the expression of *IL6* and *IL1B* was substantially attenuated by the depletion of Orai3 protein, strengthening the mechanistic link between Orai3 and inflammatory cytokine production.

DISCUSSION

The shift in ATMs toward the proinflammatory M1 phenotype is well established in rodent models of obesity (*5, 8, 9, 47*) and has also been described in humans (*48*). Thus, as expected, ATMs that we isolated from the fat pads of obese mice displayed an increased abundance of M1 cell markers and a decreased abundance of M2 cell markers (Fig. 1, A and B). Furthermore, comparison of ATMs from lean and obese mice also revealed an obesity-dependent reduction in the steady-state concentration of H$_2$S (Fig. 1, C and D).

The mechanism of H$_2$S depletion was further explored by examining the influence of inflammatory stimuli on the enzymes necessary for H$_2$S production. The abundance of CSE, but not CBS, was increased in RAW264.7 cells in response to LPS (Fig. 2C). Similarly, CSE was increased in abundance in ATMs from obese mice compared to that in ATMs from lean mice (Fig. 1F). Although the LPS-induced increase in CSE abundance was previously described (*33–35*), our major finding is that it is increased during obesity. A study showed that CSE abundance is increased by dietary restriction in a mouse model (*49*); however, this was also associated with an increased steady-state concentration of H$_2$S, which is in contrast to the data from our current study. This discrepancy reveals an interesting conundrum: the lower concentration of H$_2$S despite the increased abundance of CSE. The simplest explanation for this finding is that either H$_2$S synthesis is inhibited or H$_2$S consumption is increased under proinflammatory conditions. In our experiments, the capacity to produce H$_2$S was indeed increased by obesity (Fig. 1G) and by LPS in the presence of excess L-cysteine (Fig. 2D). Assuming the availability of an adequate amount of substrate in vivo, these data suggest that H$_2$S synthesis is not impaired by proinflammatory conditions. In contrast, the depletion of exogenous H$_2$S from the cell culture medium was enhanced when cells were stimulated with LPS, which is consistent with an increase in the consumption of H$_2$S (Fig. 2E). Whereas these data are preliminary and somewhat tangential to the primary focus of the current study, they point to increased H$_2$S consumption under proinflammatory conditions. Although this is highly speculative, we suggest that there is a role for the
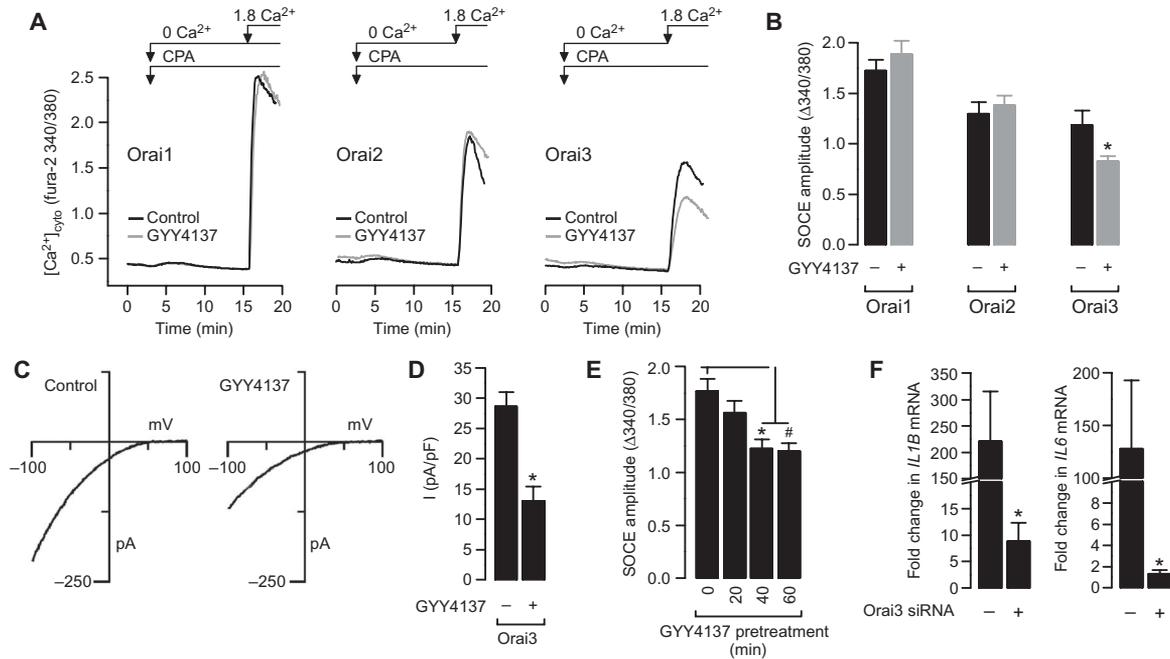
Fig. 7. GYY4137 inhibits SOCE mediated by STIM1 and Orai3 but not that mediated by STIM1 together with Orai1, or Orai2. (**A**) Typical recordings of SOCE in HEK 293 cells stably expressing STIM1 and transiently transfected with plasmids encoding Orai1, Orai2, or Orai3, as indicated. (**B**) SOCE amplitudes in HEK 293 cells expressing the indicated Orai proteins. Data are means ± SEM of six independent experiments. *P = 0.036 by unpaired t test. (**C**) Whole-cell patch clamp recordings in HEK 293 cells expressing STIM1 and Orai3 and depicting the CRAC current-voltage relationship in control cells (left) and in cells pretreated with 500 μM GYY4137 for 1 hour (right). (**D**) Summary of the peak CRAC current amplitudes measured during steps to −100 mV in the experiments depicted in (C).

Data are means ± SEM of six cells for each treatment group. *P < 0.001 by unpaired t test. (**E**) HEK 293 cells were pretreated with 500 μM GYY4137 for the indicated times before SOCE amplitudes were measured as described for Fig. 3A. Data are means ± SEM of three independent experiments. *P < 0.001 by one-way ANOVA. (**F**) RAW264.7 cells transfected with control siRNA or Orai3-specific siRNA were treated for 4 hours with LPS (1 μg/ml) and then were analyzed by qRT-PCR to determine the relative abundances of the indicated mRNAs. Data are expressed as the fold change in mRNA abundance in cells transfected with Orai3-specific siRNA compared to that in control cells. Data are means ± SEM of six independent samples. *P = 0.039, #P = 0.033 by unpaired t test.

reactive oxygen and nitrogen species that are generated during the activation of M1 macrophages. This hypothesis is based on studies that suggest that free radical species promote H_2S catabolism (50, 51). Additional studies, however, are needed to support such a model.

We observed H_2S depletion in models of both acute inflammation (LPS-treated macrophages in vitro) and chronic inflammation (ATMs from obese mice). This would suggest the involvement of a common pathway in both situations. Evidence to support this idea comes from studies of knockout mice in which loss of Toll-like receptor 4 (TLR4), a cell surface receptor for LPS, protects against insulin resistance induced by a high-fat diet (52). Furthermore, increased circulating amounts of LPS are observed in rodent models as well as in obese humans (53, 54), suggesting a direct effect of LPS in determining the shift toward an M1 phenotype in ATMs. In macrophages, TLR4-mediated signaling evokes intracellular second messenger cascades that release Ca^{2+} from stores in the ER (25, 55), which leads to a secondary Ca^{2+} influx across the plasma membrane by activation of the SOCE pathway.

As a consequence of proinflammatory signaling, either acutely induced by LPS or as a result of obesity, SOCE is increased in parallel with H_2S depletion (Figs. 3 and 6). We now propose that the reduced concentration of cellular H_2S promotes increased SOCE. In our model, H_2S is inhibitory, in that endogenous amounts appear to limit the amplitude of maximal SOCE activation. Thus, H_2S acts as a damper for SOCE. This inhibitory

input is removed when H_2S concentrations are reduced in response to proinflammatory stimuli. To support this, we showed that the application of exogenous H_2S prevented the LPS-induced increase in SOCE (Fig. 3) and reversed the effects of obesity on SOCE in ATMs (Fig. 6). Moreover, in the absence of either LPS (Fig. 4) or obesity (Fig. 6), experimentally depleting H_2S, either pharmacologically by blocking endogenous production or genetically by knocking down CSE, also increased SOCE, demonstrating that endogenous concentrations of H_2S limit maximal activation of SOCE. That being the case, it is expected that the application of exogenous H_2S alone may or may not affect SOCE depending on the preexisting steady-state concentration of H_2S. This could explain why the H_2S donor GYY4137 had no effect on SOCE in RAW264.7 cells but inhibited SOCE in mouse peritoneal macrophages (Fig. 3, C and F).

Activation of the SOCE pathway during proinflammatory stimulation provides the Ca^{2+} signal required for the activation of nuclear factor κB (NF-κB) and nuclear factor of activated T cells (NFAT), the transcription factors responsible for the expression of cytokine-encoding genes (22, 56, 57). We propose that H_2S depletion serves to amplify the proinflammatory cascade by increasing SOCE activation. We showed that inhibiting SOCE activation, either pharmacologically or genetically, attenuated the LPS-induced expression of the genes encoding the key M1 cytokines *IL6* and *IL1B* (Fig. 5). In parallel experiments, preventing H_2S depletion during LPS stimulation by inclusion of GYY4137 had qualitatively similar effects.

Thus, inhibiting SOCE or preventing the loss of H_2S both limited LPS-induced cytokine production. During obesity, we also observed the increased abundance of M1-associated markers (Figs. 1 and 6), reduced H_2S bioavailability (Fig. 1), and increased SOCE (Fig. 6) in ATMs. Similarly, inhibiting SOCE or preventing the loss of H_2S in these cells also limited proinflammatory cytokine production (Fig. 6, D to F), although the effect of these interventions was not statistically significant for all of the cytokines examined. This could be due to a lack of detection sensitivity or because the cytokine concentrations in our samples were near the lower limit of detection. Alternatively, the data could simply reflect differences in the ways in which individual cytokines are regulated by H_2S and $[Ca^{2+}]_{cyto}$. Further studies are needed to specifically examine how the H_2S-SOCE signaling axis impinges on individual proinflammatory cytokines. In addition, the potential for H_2S-SOCE signaling to regulate anti-inflammatory mediators must also be addressed. Together, our data are consistent with a model in which H_2S reduces M1-like cytokine production by inhibiting SOCE; however, we cannot state that H_2S mediates its effects exclusively through the regulation of SOCE, because H_2S is likely to affect multiple targets. Indeed, the H_2S promotes the binding of NF-κB to target genes (35), which could be a variable in our experiments.

How then does H_2S regulate SOCE in macrophages? All isoforms of STIM and Orai are found in these cells (Fig. 3G); however, we identified Orai3 as a specific target of H_2S (Fig. 7). Here, we used HEK 293 cells as a model in which to reconstitute SOCE by overexpressing STIM1 together with Orai1, Orai2, or Orai3. This approach has been widely used to investigate the functions of STIM and Orai proteins and is a useful system because of the very limited background SOCE that might otherwise complicate interpretation of the data (44–46). With this approach, we showed that the H_2S donor GYY4137 limited SOCE by inhibiting CRAC currents mediated by STIM1 and Orai3. Another advantage of using HEK 293 cells is their lack of CSE and corresponding low endogenous concentrations of H_2S, as defined previously (36). Under these conditions, we would not expect Orai3 to be constitutively modified by H_2S. This would explain the robust effect of the H_2S donor GYY4137 on SOCE and CRAC currents in these cells (Fig. 7). In contrast, we speculate that in RAW264.7 cells, which have CSE, the endogenous concentration of H_2S may be sufficiently high to constitutively modify Orai3. This might explain why GYY4137 had no effect on SOCE in these cells unless H_2S was previously depleted in response to LPS (Fig. 3C). That the magnitude of SOCE was increased in RAW264.7 cells when CSE was inhibited (Fig. 4) is also consistent with this hypothesis. In addition, Orai3-mediated SOCE was directly linked to the regulation of proinflammatory cytokine production by the observation that Orai3 was required for the robust LPS-induced expression of *IL6* and *IL1B* (Fig. 7F).

The ability of H_2S to directly modify protein function, including that of ion channels, is well documented (58). In these cases, H_2S is thought to modulate channel properties through protein sulfhydration, a process that affects protein function by modifying the sulfhydryl groups of reactive cysteine residues (58). This posttranslational modification is reported to occur over a time course of about 30 min (36), which is consistent with the time course with which GYY4137 affected SOCE function in the current study (Fig. 7E). Reactive cysteines are present in STIM (59) and Orai isoforms (60). There are four cysteine residues in the human and mouse Orai3 protein. Two of these (Cys^{101} and Cys^{118}) are conserved in Orai1 and Orai2; however, two others (Cys^{226} and Cys^{232}) are unique to Orai3 and could be potential sites for sulfhydration. The inability of GYY4137 to affect SOCE in HEK 293 cells expressing STIM1 together with Orai1 or Orai2 suggests that STIM1 is not regulated by H_2S. Regulation of STIM2, however, was not assessed in the present study and cannot be ruled out, especially because STIM2 contains a number of cysteines that are not present in

STIM1. Although our data provide insight into the mechanism by which H_2S regulates SOCE, the identification of sulfhydration of the components of SOCE and its effect on physiological function are beyond the scope of the current study.

In conclusion, our data are consistent with a model in which (i) proinflammatory conditions reduce the bioavailability of H_2S, most likely through a mechanism that involves its increased consumption; (ii) the decrease in the concentration of H_2S relieves its inhibition of Orai3, enabling the amplification of SOCE and Ca^{2+} entry; and (iii) proinflammatory cytokine production increases with the magnitude of Orai3-mediated SOCE. The potential relevance of this model is that it applies to macrophages undergoing both acute (LPS stimulation) and chronic (obesity) inflammatory responses. This would suggest that therapeutic strategies designed to maintain H_2S bioavailability or target components of the SOCE pathway could be effective in a number of pathological contexts.

MATERIALS AND METHODS

Mice
Male C57BL/6 mice (aged 4 to 6 weeks) were purchased from Taconic Biosciences Inc. and were housed in the biological resource facility at Rosalind Franklin University. For the study duration, all mice were housed with a 12-hour light-dark cycle in 12 × 6.25–inch cages with standard enrichment and ad libitum access to food and water. For studies requiring isolated peritoneal macrophages, mice were euthanized at 6 to 8 weeks of age. For obesity studies, mice were fed either a high-fat diet (D12492; 60 kcal% fat) or control diet (D12450B; 10 kcal% fat), which were purchased from Research Diets Inc. Mice were maintained on special diets from 6 weeks of age until they were euthanized at 24 to 26 weeks of age. Euthanasia was by inhalation of a lethal dose of CO_2 followed by cervical dislocation, according to the National Institutes of Health *Guide for the Care and Use of Laboratory Animals* and approved by the Institutional Animal Care and Use Committee of Rosalind Franklin University of Medicine and Science.

Cell isolation and culture
Quiescent macrophages were harvested from the mouse peritoneal cavities by aspiration according to published protocols (61). Typically, about 5 × 10^5 cells per mouse were collected in 8 ml of aspirate (phosphate-buffered saline). After centrifugation, cells were resuspended in 1 ml of serum-free Dulbecco's modified Eagle medium (DMEM; Mediatech Inc.), and 1 × 10^5 cells were plated onto 12-mm coverslips placed inside a 24-well plate. Cells were allowed to adhere for 1 hour in a tissue culture incubator before each well was washed several times with serum-free DMEM to remove non-adherent cells. It was assumed that the adherent cell population was enriched with macrophages. Cells were then incubated with experimental treatments for up to 4 hours under tissue culture conditions after which coverslips were prepared for Ca^{2+} imaging. To purify ATMs, the stromal vascular fraction (SVF) was first isolated from epididymal fat pads, as previously described (62). The macrophage population within the SVF was then extracted by immunomagnetic separation with CD11b beads (Miltenyi Biotec Inc.) according to the manufacturer's protocol. For imaging experiments, 5 × 10^4 cells were plated on each 12-mm coverslip in a 24-well plate and incubated at 37°C for 1 hour. Cells were washed with serum-free DMEM and incubated with experimental reagents for up to 4 hours before they were loaded with the fluorescent indicators fura-2AM or SF7-AM. RAW264.7 and HEK 293 cells were obtained from the American Type Culture Collection and were maintained in DMEM supplemented with 10% fetal bovine serum (Gemini Bio Products), penicillin (100 U/ml; Mediatech Inc.), and streptomycin (100 μg/ml; Mediatech Inc.) in a tissue culture incubator. For

Ca^{2+} and H$_2$S measurements, 5×10^4 cells were plated onto 12-mm coverslips the day before experimental treatments and imaging experiments were performed.

Knockdown and overexpression experiments

HEK 293 cells were transfected with plasmid encoding yellow fluorescent protein (YFP)–tagged STIM1 (STIM1-YFP), and a stably expressing population of cells was selected with puromycin. For Ca^{2+} imaging experiments, the HEK 293 STIM1-YFP stable cell line was transiently transfected with plasmids encoding cyan fluorescent protein (CFP)–tagged Orai1, Orai2, or Orai3 with a Nucleofector device (Lonza Inc.), and experiments were performed 24 to 48 hours later. Stable knockdown of CSE in RAW264.7 cells was performed by transduction with lentivirus encoding control or CSE-specific shRNA (Santa Cruz Biotechnology Inc.) and selection in puromycin. Transient knockdown of proteins in RAW264.7 cells was achieved by nucleofection with control, Orai3-specific, or STIM1-specific siRNAs (obtained from Santa Cruz Biotechnology Inc.) 24 to 48 hours before experiments were performed.

Intracellular Ca^{2+} measurement

Cells cultured on glass coverslips were loaded with 2 μM fura-2AM (Life Technologies) by incubation at room temperature for 45 min and then were mounted in a recording chamber positioned on the stage of an inverted fluorescence microscope (IX71, Olympus America Inc.). Fura-2 was alternately excited at 340 and 380 nm, and the emitted fluorescence filtered at 510 nm was collected and recorded with a charge-coupled device–based imaging system running SimplePCI software (Hamamatsu Photonics). Cytoplasmic [Ca^{2+}] is reported as the ratio of background-corrected fluorescence intensity at 340 and 380 nm. The chamber was continuously perfused with Hank's balanced salt solution (HBSS) containing 137.9 mM NaCl, 5.33 mM KCl, 0.44 mM KH$_2$PO$_4$, 0.34 mM Na$_2$HPO$_4$, 5.56 mM glucose, 4.17 mM NaHCO$_3$, 1.8 mM CaCl$_2$, 0.49 mM MgCl$_2$, 0.41 mM MgSO$_4$, 10 mM Hepes (pH 7.4) with NaOH. To prepare a Ca^{2+}-free solution, CaCl$_2$ was substituted with MgCl$_2$ and 1 mM EGTA was added. A solution changer was used to switch the composition of the solution bathing the cells under study.

Measurement of H$_2$S

The concentration of cytoplasmic H$_2$S was monitored with SF7-AM, which was synthesized by C. Chang (University of California, Berkeley), as described previously (31). RAW264.7 cells or freshly isolated ATMs were plated at 5×10^4 cells per well in an optical flat-bottomed 96-well plate and were loaded with SF7-AM (2 μM for RAW264.7 cells and 0.5 μM for ATMs) and incubated at 37°C for 45 min (RAW264.7 cells) or 30 min (ATMs). After incubation, the wells were washed with HBSS, the plate was placed on the stage of a fluorescence microscope, and images were captured with excitation and emission wavelengths of 490 and 525 nm, respectively. The capacity of cells and tissues to produce H$_2$S was monitored with the methylene blue assay, as previously described (36). Cell or tissue lysates suspended in 10 mM potassium phosphate buffer (pH 7.4) were transferred to high-performance liquid chromatography injection vials. Pyridoxal 5′ phosphate (2 mM) and L-cysteine (10 mM) were added, and the air was replaced with nitrogen before sealing. The vials were incubated for 2 hours at 37°C before zinc acetate was injected, which was followed by a further 1 hour of incubation. Finally, 20 mM N,N-dimethyl-p-phenylenediamine sulfate in 7.2 M HCl was injected, which was followed by FeCl$_3$ in 1.2 M HCl, and the absorbance at 650 nm was measured after 20 min.

Whole-cell patch clamp recordings

Patch clamp recordings were performed with an Axopatch 200B amplifier (Molecular Devices LLC) interfaced to an ITC-18 input/output board and an iMac G5 computer, as described previously (45). Currents were filtered at 1 kHz with a four-pole Bessel filter and were sampled at 5 kHz. The holding potential was +30 mV. The voltage protocol consisted of a 100-ms step to −100 mV from the holding potential followed by a ramp (100 ms) from −100 to +100 mV repeated every 1 s. HEK 293 cells stably expressing STIM1 were transiently transfected with plasmid encoding CFP-Orai3 (500 ng per 12-mm coverslip) with TransPass D2 (New England Biolabs Inc.). During recording, cells were bathed in solution containing 130 mM NaCl, 4.5 mM KCl, 20 mM CaCl$_2$, 10 mM D-glucose, and 5 mM Na-Hepes (pH 7.4). Tetraethylammonium chloride (10 mM) was added to all extracellular solutions to prevent contamination from voltage-gated K$^+$ channels. The standard internal solution contained 135 mM cesium aspartate, 8 mM MgCl$_2$, 8 mM BAPTA [1,2-bis(2-aminophenoxy)ethane-N,N,N,N-tetraacetic acid], and 8 mM Cs-Hepes (pH 7.2). All data were corrected for leak currents collected in 20 mM Ca^{2+} and 100 μM La^{3+}.

qRT-PCR analysis and measurement of cytokine production

To evaluate the expression of genes encoding M1 and M2 markers, total cellular RNA was extracted from ATMs after homogenization in TRIzol reagent (Life Technologies), according to the manufacturer's protocol. Two micrograms of total RNA was used as a template for complementary DNA synthesis with random primers and the M-MLV Reverse Transcriptase system (Life Technologies). Duplex qRT-PCR analysis was performed with the StepOne real-time PCR system (Life Technologies). Assays were performed in duplicate, and semiquantitative analysis of gene expression was performed with the comparative threshold method. Gene expression analysis (relative to internal standards GAPDH or HPRT1) was performed with prevalidated TaqMan gene expression assays (Life Technologies) for NOS2, ITGAX, MRC1, ARG1, Chil3, and SYBR Green PCR Master Mix (Applied Biosystems) with validated primers for IL6 and IL1B. The secretion of the mouse proinflammatory cytokines TNF-α, IL-6, and IL-1β by ATMs into the culture medium was analyzed in duplicate with the MILLIPLEX MAP kit (Millipore) and assayed on a MAGPIX instrument (Luminex Corp.) according to the manufacturer's instructions.

Reagents

GYY4137 dichloromethane, CPA, LPS, PPG, AOAA, and antibody against Orai1 were obtained from Sigma-Aldrich. Antibody against STIM1 was purchased from Santa Cruz Biotechnology Inc., and antibodies against STIM2, Orai2, and Orai3 were obtained from ProSci Inc. The CFP-Orai2 and CFP-Orai3 expression plasmids were gifts from J. Putney (National Institute of Environmental Health Sciences, Research Triangle Park, NC), and the CFP-Orai1 and YFP-STIM1 constructs were gifts from A. Rao (Addgene plasmids 19757 and 19754, respectively).

Statistical analysis

Fluorescence imaging data were collected with a 20× objective lens, enabling capture of ~50 cells per image field. Multiple image fields were acquired from each coverslip or well of a 96-well plate, and the data were pooled from three or four independent coverslips or wells acquired on at least two different days from independent cultures or at least three animals. All fluorescence intensities were background-subtracted. Normally distributed data were summarized as means ± SEM, and differences between means were assessed with the Student's t test for unpaired comparisons. A one-way ANOVA with Fisher's least significant difference post hoc analysis was used for multiple comparisons. Where data are presented as percentages relative to control values, statistical analysis was performed before the data were normalized. For all tests, the differences between means were accepted as statistically significant at the 95% level ($P < 0.05$).

SUPPLEMENTARY MATERIALS

www.sciencesignaling.org/cgi/content/full/8/407/ra128/DC1
Fig. S1. LPS increases the abundance of CSE but not CBS.
Fig. S2. LPS has no effect on the abundances of STIM and Orai isoforms.
Fig. S3. Inhibition of endogenous H_2S production increases SOCE.
Fig. S4. Analysis of the knockdown of STIM1 in RAW264.7 cells.
Fig. S5. SOCE is enhanced in ATMs from obese mice.
Fig. S6. Western blotting analysis of STIM1-YFP and Orai-CFP proteins in transfected HEK 293 cells.
Fig. S7. Analysis of the knockdown of Orai3 in RAW264.7 cells.

REFERENCES AND NOTES

1. M. A. Albert, R. J. Glynn, P. M. Ridker, Plasma concentration of C-reactive protein and the calculated Framingham Coronary Heart Disease Risk score. *Circulation* **108**, 161–165 (2003).
2. G. S. Hotamisligil, N. S. Shargill, B. M. Spiegelman, Adipose expression of tumor necrosis factor-alpha: Direct role in obesity-linked insulin resistance. *Science* **259**, 87–91 (1993).
3. G. S. Hotamisligil, P. Arner, J. F. Caro, R. L. Atkinson, B. M. Spiegelman, Increased adipose tissue expression of tumor necrosis factor-α in human obesity and insulin resistance. *J. Clin. Invest.* **95**, 2409–2415 (1995).
4. J. Hirosumi, G. Tuncman, L. Chang, C. Z. Görgün, K. T. Uysal, K. Maeda, M. Karin, G. S. Hotamisligil, A central role for JNK in obesity and insulin resistance. *Nature* **420**, 333–336 (2002).
5. H. Xu, G. T. Barnes, Q. Yang, G. Tan, D. Yang, C. J. Chou, J. Sole, A. Nichols, J. S. Ross, L. A. Tartaglia, H. Chen, Chronic inflammation in fat plays a crucial role in the development of obesity-related insulin resistance. *J. Clin. Invest.* **112**, 1821–1830 (2003).
6. A. D. Pradhan, J. E. Manson, N. Rifai, J. E. Buring, P. M. Ridker, C-reactive protein, interleukin 6, and risk of developing type 2 diabetes mellitus. *JAMA* **286**, 327–334 (2001).
7. G. Luc, J.-M. Bard, I. Juhan-Vague, J. Ferrieres, A. Evans, P. Amouyel, D. Arveiler, J.-C. Fruchart, P. Ducimetiere, C-reactive protein, interleukin-6, and fibrinogen as predictors of coronary heart disease: The PRIME Study. *Arterioscler. Thromb. Vasc. Biol.* **23**, 1255–1261 (2003).
8. S. P. Weisberg, D. McCann, M. Desai, M. Rosenbaum, R. L. Leibel, A. W. Ferrante Jr., Obesity is associated with macrophage accumulation in adipose tissue. *J. Clin. Invest.* **112**, 1796–1808 (2003).
9. C. N. Lumeng, S. M. DeYoung, J. L. Bodzin, A. R. Saltiel, Increased inflammatory properties of adipose tissue macrophages recruited during diet-induced obesity. *Diabetes* **56**, 16–23 (2007).
10. L. Li, M. Salto-Tellez, C.-H. Tan, M. Whiteman, P. K. Moore, GYY4137, a novel hydrogen sulfide-releasing molecule, protects against endotoxic shock in the rat. *Free Radic. Biol. Med.* **47**, 103–113 (2009).
11. N. Dufton, J. Natividad, E. F. Verdu, J. L. Wallace, Hydrogen sulfide and resolution of acute inflammation: A comparative study utilizing a novel fluorescent probe. *Sci. Rep.* **2**, 499 (2012).
12. L.-F. Hu, P. T.-H. Wong, P. K. Moore, J.-S. Bian, Hydrogen sulfide attenuates lipopolysaccharide-induced inflammation by inhibition of p38 mitogen-activated protein kinase in microglia. *J. Neurochem.* **100**, 1121–1128 (2007).
13. M. Whiteman, L. Li, P. Rose, C.-H. Tan, D. B. Parkinson, P. K. Moore, The effect of hydrogen sulfide donors on lipopolysaccharide-induced formation of inflammatory mediators in macrophages. *Antioxid. Redox Signal.* **12**, 1147–1154 (2010).
14. S. Faller, K. K. Zimmermann, K. M. Strosing, H. Engelstaedter, H. Buerkle, R. Schmidt, S. G. Spassov, A. Hoetzel, Inhaled hydrogen sulfide protects against lipopolysaccharide-induced acute lung injury in mice. *Med. Gas Res.* **2**, 26 (2012).
15. M. Whiteman, P. G. Winyard, Hydrogen sulfide and inflammation: The good, the bad, the ugly and the promising. *Expert Rev. Clin. Pharmacol.* **4**, 13–32 (2011).
16. H. Zhang, C. Guo, D. Wu, A. Zhang, T. Gu, L. Wang, C. Wang, Hydrogen sulfide inhibits the development of atherosclerosis with suppressing CX3CR1 and CX3CL1 expression. *PLOS One* **7**, e41147 (2012).
17. S. K. Jain, R. Bull, J. L. Rains, P. F. Bass, S. N. Levine, S. Reddy, R. McVie, J. A. Bocchini Jr., Low levels of hydrogen sulfide in the blood of diabetes patients and streptozotocin-treated rats causes vascular inflammation? *Antioxid. Redox Signal.* **12**, 1333–1337 (2010).
18. V. Brancaleone, F. Roviezzo, V. Vellecco, L. De Gruttola, M. Bucci, G. Cirino, Biosynthesis of H_2S is impaired in non-obese diabetic (NOD) mice. *Br. J. Pharmacol.* **155**, 673–680 (2008).
19. K. Suzuki, G. Olah, K. Modis, C. Coletta, G. Kulp, D. Gerö, P. Szoleczky, T. Chang, Z. Zhou, L. Wu, R. Wang, A. Papapetropoulos, C. Szabo, Hydrogen sulfide replacement therapy protects the vascular endothelium in hyperglycemia by preserving mitochondrial function. *Proc. Natl. Acad. Sci. U.S.A.* **108**, 13829–13834 (2011).
20. M. Whiteman, K. M. Gooding, J. L. Whatmore, C. I. Ball, D. Mawson, K. Skinner, J. E. Tooke, A. C. Shore, Adiposity is a major determinant of plasma levels of the novel vasodilator hydrogen sulphide. *Diabetologia* **53**, 1722–1726 (2010).
21. L. Martin, S. C. Pingle, D. M. Hallam, L. P. Rybak, V. Ramkumar, Activation of the adenosine A_3 receptor in RAW 264.7 cells inhibits lipopolysaccharide-stimulated tumor necrosis factor-α release by reducing calcium-dependent activation of nuclear factor-κB and extracellular signal-regulated kinase 1/2. *J. Pharmacol. Exp. Ther.* **316**, 71–78 (2006).
22. X. Zhou, W. Yang, J. Li, Ca^{2+}- and protein kinase C-dependent signaling pathway for nuclear factor-κB activation, inducible nitric-oxide synthase expression, and tumor necrosis factor-α production in lipopolysaccharide-stimulated rat peritoneal macrophages. *J. Biol. Chem.* **281**, 31337–31347 (2006).
23. G. Chen, S. Panicker, K.-Y. Lau, S. Apparsundaram, V. A. Patel, S.-L. Chen, R. Soto, J. K. C. Jung, P. Ravindran, D. Okuhara, G. Bohnert, Q. Che, P. E. Rao, J. D. Allard, L. Badi, H.-M. Bitter, P. A. Nunn, S. K. Narula, J. A. DeMartino, Characterization of a novel CRAC inhibitor that potently blocks human T cell activation and effector functions. *Mol. Immunol.* **54**, 355–367 (2013).
24. Y. Ye, Y. Zhang, X. Lu, X. Huang, X. Zeng, X. Lai, Y. Zeng, The anti-inflammatory effect of the SOCC blocker SK&F 96365 on mouse lymphocytes after stimulation by Con A or PMA/ionomycin. *Immunobiology* **216**, 1044–1053 (2011).
25. S.-W. Jin, L. Zhang, Q.-Q. Lian, S.-L. Yao, P. Wu, X.-Y. Zhou, W. Xiong, D.-Y. Ye, Close functional coupling between Ca^{2+} release-activated Ca^{2+} channels and reactive oxygen species production in murine macrophages. *Mediators Inflamm.* **2006**, 36192 (2006).
26. S. Feske, ORAI1 and STIM1 deficiency in human and mice: Roles of store-operated Ca^{2+} entry in the immune system and beyond. *Immunol. Rev.* **231**, 189–209 (2009).
27. L. Navarro-Borelly, A. Somasundaram, M. Yamashita, D. Ren, R. J. Miller, M. Prakriya, STIM1–Orai1 interactions and Orai1 conformational changes revealed by live-cell FRET microscopy. *J. Physiol.* **586**, 5383–5401 (2008).
28. C. Y. Park, P. J. Hoover, F. M. Mullins, P. Bachhawat, E. D. Covington, S. Raunser, T. Walz, K. C. Garcia, R. E. Dolmetsch, R. S. Lewis, STIM1 clusters and activates CRAC channels via direct binding of a cytosolic domain to Orai1. *Cell* **136**, 876–890 (2009).
29. M. M. Wu, J. Buchanan, R. M. Luik, R. S. Lewis, Ca^{2+} store depletion causes STIM1 to accumulate in ER regions closely associated with the plasma membrane. *J. Cell Biol.* **174**, 803–813 (2006).
30. L. Munaron, D. Avanzato, F. Moccia, D. Mancardi, Hydrogen sulfide as a regulator of calcium channels. *Cell Calcium* **53**, 77–84 (2013).
31. V. S. Lin, A. R. Lippert, C. J. Chang, Cell-trappable fluorescent probes for endogenous hydrogen sulfide signaling and imaging H_2O_2-dependent H_2S production. *Proc. Natl. Acad. Sci. U.S.A.* **110**, 7131–7135 (2013).
32. V. S. Lin, W. Chen, M. Xian, C. J. Chang, Chemical probes for molecular imaging and detection of hydrogen sulfide and reactive sulfur species in biological systems. *Chem. Soc. Rev.* **44**, 4596–4618 (2015).
33. L. Li, M. Bhatia, Y. Z. Zhu, Y. C. Zhu, R. D. Ramnath, Z. J. Wang, F. B. M. Anuar, M. Whiteman, M. Salto-Tellez, P. K. Moore, Hydrogen sulfide is a novel mediator of lipopolysaccharide-induced inflammation in the mouse. *FASEB J.* **19**, 1196–1198 (2005).
34. G.-S. Oh, H.-O. Pae, B.-S. Lee, B.-N. Kim, J.-M. Kim, H.-R. Kim, S. B. Jeon, W. K. Jeon, H.-J. Chae, H.-T. Chung, Hydrogen sulfide inhibits nitric oxide production and nuclear factor-κB via heme oxygenase-1 expression in RAW264.7 macrophages stimulated with lipopolysaccharide. *Free Radic. Biol. Med.* **41**, 106–119 (2006).
35. N. Sen, B. D. Paul, M. M. Gadalla, A. K. Mustafa, T. Sen, R. Xu, S. Kim, S. H. Snyder, Hydrogen sulfide-linked sulfhydration of NF-κB mediates its antiapoptotic actions. *Mol. Cell* **45**, 13–24 (2012).
36. A. K. Mustafa, M. M. Gadalla, N. Sen, S. Kim, W. Mu, S. K. Gazi, R. K. Barrow, G. Yang, R. Wang, S. H. Snyder, H_2S signals through protein S-sulfhydration. *Sci. Signal.* **2**, ra72 (2009).
37. L. Li, M. Whiteman, Y. Y. Guan, K. L. Neo, Y. Cheng, S. W. Lee, Y. Zhao, R. Baskar, C.-H. Tan, P. K. Moore, Characterization of a novel, water-soluble hydrogen sulfide–releasing molecule (GYY4137): New insights into the biology of hydrogen sulfide. *Circulation* **117**, 2351–2360 (2008).
38. G. S. Bird, W. I. DeHaven, J. T. Smyth, J. W. Putney Jr., Methods for studying store-operated calcium entry. *Methods* **46**, 204–212 (2008).
39. M. I. Lioudyno, J. A. Kozak, A. Penna, O. Safrina, S. L. Zhang, D. Sen, J. Roos, K. A. Stauderman, M. D. Cahalan, Orai1 and STIM1 move to the immunological synapse and are up-regulated during T cell activation. *Proc. Natl. Acad. Sci. U.S.A.* **105**, 2011–2016 (2008).
40. X.-Y. Zhu, S.-J. Liu, Y.-J. Liu, S. Wang, X. Ni, Glucocorticoids suppress cystathionine gamma-lyase expression and H_2S production in lipopolysaccharide-treated macrophages. *Cell. Mol. Life Sci.* **67**, 1119–1132 (2010).
41. A. Asimakopoulou, P. Panopoulos, C. T. Chasapis, C. Coletta, Z. Zhou, G. Cirino, A. Giannis, C. Szabo, G. A. Spyroulias, A. Papapetropoulos, Selectivity of commonly used pharmacological inhibitors for cystathionine β synthase (CBS) and cystathionine γ lyase (CSE). *Br. J. Pharmacol.* **169**, 922–932 (2013).
42. C. Zitt, B. Strauss, E. C. Schwarz, N. Spaeth, G. Rast, A. Hatzelmann, M. Hoth, Potent inhibition of Ca^{2+} release-activated Ca^{2+} channels and T-lymphocyte activation by the pyrazole derivative BTP2. *J. Biol. Chem.* **279**, 12427–12437 (2004).

43. Y. Wang, X. Deng, Y. Zhou, E. Hendron, S. Mancarella, M. F. Ritchie, X. D. Tang, Y. Baba, T. Kurosaki, Y. Mori, J. Soboloff, D. L. Gill, STIM protein coupling in the activation of Orai channels. *Proc. Natl. Acad. Sci. U.S.A.* **106**, 7391–7396 (2009).

44. W. I. DeHaven, J. T. Smyth, R. R. Boyles, J. W. Putney Jr., Calcium inhibition and calcium potentiation of Orai1, Orai2, and Orai3 calcium release-activated calcium channels. *J. Biol. Chem.* **282**, 17548–17556 (2007).

45. M. Yamashita, L. Navarro-Borelly, B. A. McNally, M. Prakriya, Orai1 mutations alter ion permeation and Ca^{2+}-dependent fast inactivation of CRAC channels: Evidence for coupling of permeation and gating. *J. Gen. Physiol.* **130**, 525–540 (2007).

46. J. Soboloff, M. A. Spassova, X. D. Tang, T. Hewavitharana, W. Xu, D. L. Gill, Orai1 and STIM reconstitute store-operated calcium channel function. *J. Biol. Chem.* **281**, 20661–20665 (2006).

47. C. N. Lumeng, J. L. Bodzin, A. R. Saltiel, Obesity induces a phenotypic switch in adipose tissue macrophage polarization. *J. Clin. Invest.* **117**, 175–184 (2007).

48. J. M. Wentworth, G. Naselli, W. A. Brown, L. Doyle, B. Phipson, G. K. Smyth, M. Wabitsch, P. E. O'Brien, L. C. Harrison, Pro-inflammatory CD11c⁺CD206⁺ adipose tissue macrophages are associated with insulin resistance in human obesity. *Diabetes* **59**, 1648–1656 (2010).

49. C. Hine, E. Harputlugil, Y. Zhang, C. Ruckenstuhl, B. C. Lee, L. Brace, A. Longchamp, J. H. Treviño-Villarreal, P. Mejia, C. K. Ozaki, R. Wang, V. N. Gladyshev, F. Madeo, W. B. Mair, J. R. Mitchell, Endogenous hydrogen sulfide production is essential for dietary restriction benefits. *Cell* **160**, 132–144 (2015).

50. S. Carballal, M. Trujillo, E. Cuevasanta, S. Bartesaghi, M. N. Möller, L. K. Folkes, M. A. García-Bereguiaín, C. Gutiérrez-Merino, P. Wardman, A. Denicola, R. Radi, B. Alvarez, Reactivity of hydrogen sulfide with peroxynitrite and other oxidants of biological interest. *Free Radic. Biol. Med.* **50**, 196–205 (2011).

51. A. Stein, S. M. Bailey, Redox biology of hydrogen sulfide: Implications for physiology, pathophysiology, and pharmacology. *Redox Biol.* **1**, 32–39 (2013).

52. J. E. Davis, N. K. Gabler, J. Walker-Daniels, M. E. Spurlock, Tlr-4 deficiency selectively protects against obesity induced by diets high in saturated fat. *Obesity* **16**, 1248–1255 (2008).

53. P. D. Cani, J. Amar, M. A. Iglesias, M. Poggi, C. Knauf, D. Bastelica, A. M. Neyrinck, F. Fava, K. M. Tuohy, C. Chabo, A. Waget, E. Delmée, B. Cousin, T. Sulpice, B. Chamontin, J. Ferrières, J.-F. Tanti, G. R. Gibson, L. Casteilla, N. M. Delzenne, M. C. Alessi, R. Burcelin, Metabolic endotoxemia initiates obesity and insulin resistance. *Diabetes* **56**, 1761–1772 (2007).

54. S. Basu, M. Haghiac, P. Surace, J.-C. Challier, M. Guerre-Millo, K. Singh, T. Waters, J. Minium, L. Presley, P. M. Catalano, S. Hauguel-de Mouzon, Pregravid obesity associates with increased maternal endotoxemia and metabolic inflammation. *Obesity* **19**, 476–482 (2011).

55. D. Aki, Y. Minoda, H. Yoshida, S. Watanabe, R. Yoshida, G. Takaesu, T. Chinen, T. Inaba, M. Hikida, T. Kurosaki, K. Saeki, A. Yoshimura, Peptidoglycan and lipopolysaccharide activate PLCγ2, leading to enhanced cytokine production in macrophages and dendritic cells. *Genes Cells* **13**, 199–208 (2008).

56. O. Letari, S. Nicosia, C. Chiavaroli, P. Vacher, W. Schlegel, Activation by bacterial lipopolysaccharide causes changes in the cytosolic free calcium concentration in single peritoneal macrophages. *J. Immunol.* **147**, 980–983 (1991).

57. Y. Kim, J. S. Moon, K. S. Lee, S. Y. Park, J. Cheong, H. S. Kang, H. Y. Lee, H. D. Kim, Ca^{2+}/calmodulin-dependent protein phosphatase calcineurin mediates the expression of iNOS through IKK and NF-κB activity in LPS-stimulated mouse peritoneal macrophages and RAW 264.7 cells. *Biochem. Biophys. Res. Commun.* **314**, 695–703 (2004).

58. B. D. Paul, S. H. Snyder, H2S signalling through protein sulfhydration and beyond. *Nat. Rev. Mol. Cell Biol.* **13**, 499–507 (2012).

59. B. J. Hawkins, K. M. Irrinki, K. Mallilankaraman, Y.-C. Lien, Y. Wang, C. D. Bhanumathy, R. Subbiah, M. F. Ritchie, J. Soboloff, Y. Baba, T. Kurosaki, S. K. Joseph, D. L. Gill, M. Madesh, S-glutathionylation activates STIM1 and alters mitochondrial homeostasis. *J. Cell Biol.* **190**, 391–405 (2010).

60. I. Bogeski, R. Kappl, C. Kummerow, R. Gulaboski, M. Hoth, B. A. Niemeyer, Redox regulation of calcium ion channels: Chemical and physiological aspects. *Cell Calcium* **50**, 407–423 (2011).

61. X. Zhang, R. Goncalves, D. M. Mosser, The isolation and characterization of murine macrophages. *Curr. Protoc. Immunol.* **Chapter 14**, Unit 14.1 (2008).

62. J. S. Orr, A. J. Kennedy, A. H. Hasty, Isolation of adipose tissue immune cells. *J. Vis. Exp.* e50707 (2013).

Science Signaling

Depletion of H$_2$S during obesity enhances store-operated Ca^{2+} entry in adipose tissue macrophages to increase cytokine production

Gopal V. Velmurugan, Huiya Huang, Hongbin Sun, Joseph Candela, Mukesh K. Jaiswal, Kenneth D. Beaman, Megumi Yamashita, Murali Prakriya and Carl White

Limiting inflammation in obesity

Obese individuals have increased amounts of inflammatory cytokines in the circulation, which are produced by adipose tissue macrophages (ATMs). Velmurugan *et al.* found that ATMs from obese mice had decreased amounts of the gaseous signaling molecule hydrogen sulfide (H$_2$S) than did ATMs from lean mice. ATMs from obese mice had enhanced store-operated calcium entry and produced more proinflammatory cytokines. Treatment of macrophages with the bacterial product lipopolysaccharide also decreased H$_2$S concentrations and increased inflammatory cytokine production. Knockdown experiments showed that H$_2$S inhibited the channel protein Orai3 to reduce calcium entry into macrophages. Together, these data suggest that inflammatory stimuli lead to the depletion of H$_2$S in adipose tissue, which exacerbates inflammatory responses by resident ATMs.

ARTICLE TOOLS	http://stke.sciencemag.org/content/8/407/ra128
SUPPLEMENTARY MATERIALS	http://stke.sciencemag.org/content/suppl/2015/12/11/8.407.ra128.DC1
RELATED CONTENT	http://stke.sciencemag.org/content/sigtrans/8/407/pc30.full http://stke.sciencemag.org/content/sigtrans/5/251/ra85.full http://stke.sciencemag.org/content/sigtrans/8/373/ra37.full http://stke.sciencemag.org/content/sigtrans/7/342/ra87.full http://science.sciencemag.org/content/sci/347/6217/26.full http://science.sciencemag.org/content/sci/350/6257/161.full http://stm.sciencemag.org/content/scitransmed/6/247/247ra103.full http://stke.sciencemag.org/content/sigtrans/9/418/ra26.full http://stke.sciencemag.org/content/sigtrans/9/418/pc6.full http://stke.sciencemag.org/content/sigtrans/9/418/eg3.full http://stke.sciencemag.org/content/sigtrans/9/422/ec83.abstract http://stke.sciencemag.org/content/sigtrans/9/424/ec94.abstract http://stke.sciencemag.org/content/sigtrans/9/441/ra80.full http://stke.sciencemag.org/content/sigtrans/10/505/eaar4569.full
REFERENCES	This article cites 60 articles, 21 of which you can access for free http://stke.sciencemag.org/content/8/407/ra128#BIBL

Use of this article is subject to the Terms of Service

Use of this article is subject to the Terms of Service